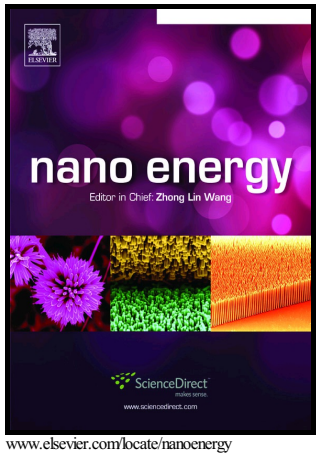

www.elsevier.com/locate/nanoenergy

Ultra-High Thermoelectric Performance in Graphene Incorporated Cu_2Se: Role of Mismatching Phonon Modes

Meng Li, David L. Cortie, Jixing Liu, Dehong Yu, Sheik Md. Kazi Nazrul Islam, Lanling Zhao, David R.G. Mitchell, Richard A. Mole, Michael B. Cortie, Shixue Dou, Xiaolin Wang

PII: S2211-2855(18)30685-2
DOI: https://doi.org/10.1016/j.nanoen.2018.09.041
Reference: NANOEN3046

To appear in: *Nano Energy*

Received date: 29 August 2018
Accepted date: 17 September 2018

Cite this article as: Meng Li, David L. Cortie, Jixing Liu, Dehong Yu, Sheik Md. Kazi Nazrul Islam, Lanling Zhao, David R.G. Mitchell, Richard A. Mole, Michael B. Cortie, Shixue Dou and Xiaolin Wang, Ultra-High Thermoelectric Performance in Graphene Incorporated Cu_2Se: Role of Mismatching Phonon Modes, *Nano Energy,* https://doi.org/10.1016/j.nanoen.2018.09.041

Ultra-High Thermoelectric Performance in Graphene Incorporated Cu_2Se: Role of Mismatching Phonon Modes

Meng Li[a, 1], David L Cortie[a, *], Jixing Liu[a, b, c], Dehong Yu[d], Sheik Md. Kazi Nazrul Islam[a], Lanling Zhao[a, e], David R. G. Mitchell[f], Richard A. Mole[d], Michael B Cortie[g], Shixue Dou[a], Xiaolin Wang[a, *]

[a] *Institute for Superconducting and Electronic Materials, Australian Institute for Innovative Materials, University of Wollongong, North Wollongong, NSW 2500, Australia*

[b] *School of Material Science and Engineering, Northeastern University, Shenyang, 110819, China*

[c] *Superconducting Materials Research Center, Northwest Institute for Nonferrous Metal Research, Xian, 710016, China*

[d] *Australian Nuclear Science and Technology Organization, Lucas Heights, Menai, NSW*

[e] School of Physics, Shandong University, Jinan, Shandong 250100, P. R. China

[f] *Electron Microscopy Centre, Australian Institute for Innovative Materials, University of Wollongong, North Wollongong, NSW 2500, Australia*

[g] *School of Mathematical and Physical Sciences, University of Technology Sydney, PO Box 123, Broadway, NSW 2007, Australia*

† xiaolin@uow.edu.au

‡ dcortie@uow.edu.au

Abstract

A thermoelectric material consisting of Cu_2Se incorporated with up to 0.45 wt% of graphene nanoplates is reported. The carbon-reinforced Cu_2Se exhibits an ultra-high thermoelectric figure-of-merit of zT = 2.44 ± 0.25 at 870 K. Microstructural characterization reveals dense, nanostructured grains of Cu_2Se with multilayer-graphene and graphite agglomerations located at grain boundaries. High temperature X-ray diffraction shows that the graphene incorporated Cu_2Se matrix retains a cubic structure and the composite microstructure is chemically stable. Based on the experimental structure, density functional theory was used to calculate the formation energy of carbon point defects and the associated phonon density of states. The isolated carbon inclusion is shown to have a high formation energy in Cu_2Se whereas graphene and graphite phases are enthalpically stable relative to the solid solution. Neutron

spectroscopy proves that there is a frequency mismatch in the phonon density of states between the carbon honeycomb phases and cubic Cu_2Se. This provides a mechanism for the strong scattering of phonons at the composite interfaces, which significantly impedes the conduction of heat and enhances thermoelectric performance.

Graphical abstract

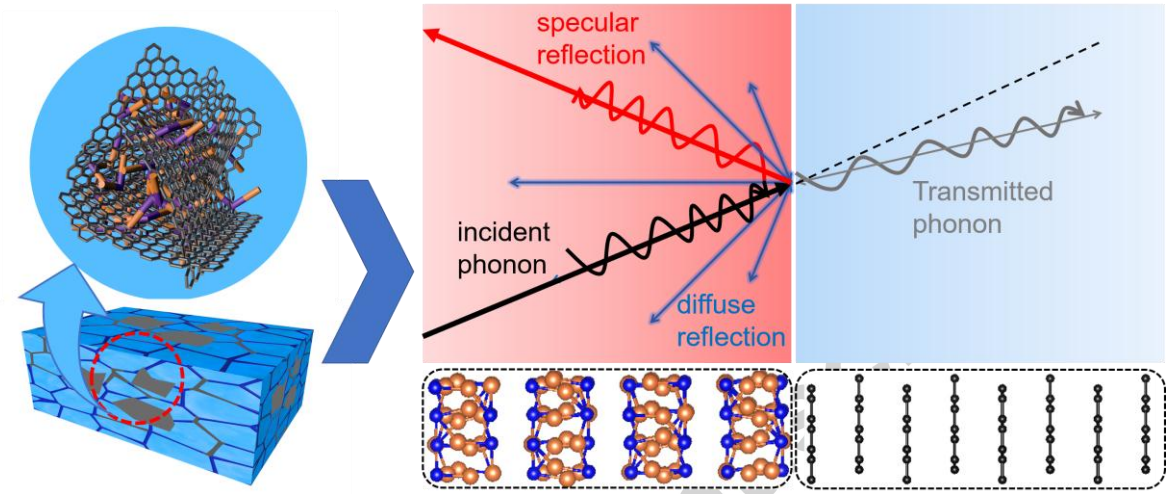

Keyword

Thermoelectric; Cu_2Se/graphene nanocomposite; interfacial thermal resistance; density functional theory.

1. Introduction

Thermoelectric (TE) materials offer an attractive augmentation in high-temperature devices because they provide a mechanism to capture and recycle waste-heat into electricity.[1–7] In the past decades, promising developments have inspired hope that the next-generation of advanced thermoelectrics could play an increasing role in sustainable technology.[8–11] In order to compare the efficiency of different thermoelectric materials, Ioffe defined the figure-of-merit (zT), as $zT = S^2\sigma T/\kappa$, where S, σ, T and κ are the Seebeck coefficient, electrical conductivity, absolute temperature and thermal conductivity, respectively.[12,13] In many cases, achieving low κ becomes the decisive factor for optimizing thermoelectric performance because there are strong competing correlations between S and σ that make it difficult to

modulate the power factor ($S^2\sigma$).[14,15] Recently, there has been renewed interest in the superionic conductors in the cuprous selenide (Cu_2Se) family because they present a promising figure-of-merit at high temperatures (~1000 K) enabled by the low thermal conductivity.[16,17] The origin of the low thermal conductivity remains debated, however, it is generally believed that either strong anharmonic interactions in the lattice-phonon system,[18] or the liquid-like motion of the Cu ions are responsible for impeding phonon transport. Despite the promising performance, practical applications of these materials have been hindered by the chemical complications associated with Cu phase segregation, and in tandem, *zT* is too low to be competitive in the critical temperature region between 400 K and 900 K.[19]

Various strategies have been employed to enhance the *zT* and the chemical stability of Cu_2Se over a broad temperature range. A facile method is chemical doping via the addition of transition metals (Ag, Fe, Mn,)[20,21] or alkaline elements (Li, Na, K, Mg)[22] to replace Cu, or halogen or chalcogen elements (I, S, Te)[23–25] to replace Se. Other novel concepts include grain boundary engineering,[26,27] the formation of high entropy alloys[28] and design of nanocomposites.[29] The formation of composites based on *hierarchical* microstructures containing a primary matrix phase embedded with secondary-phase inclusions spanning spatial scales from the micrometer scale down to the nanoscale has also proven to be a generally effective route to optimize thermoelectrics.[30,31] Very recently, a large increase in performance for Cu_2Se was reported by two groups, including our own, using a doping strategy based on incorporating secondary carbon phases such as carbon fiber, carbon graphite powder, black carbon or carbon nanotubes into the Cu_2Se matrix.[32,33] The inclusion of light low-atomic mass carbon nanostructures increases *zT* for Cu_2Se up to 2.4 in the temperature range below 1000 K. Despite the enticing opportunities offered by these carbon-based Cu_2Se composites, many open questions still remain concerning the underlying chemical and phonon mechanisms. It is essential to resolve these questions and reveal the optimal doping route for superior thermoelectric performance.

Our recent work on carbon Cu_2Se nanocomposites, based on several different carbon precursors including carbon graphite and carbon fibre, demonstrated some universal features across the entire family of hybrid materials. In every case, the thermal conductivity κ was reduced with the addition of carbon, although different carbon precursors led to a variable reduction of the electrical conductivity in the end product. Secondary carbon phases were

embedded in the Cu_2Se matrix detected by transmission electron microscopy, implying low chemical reactivity between the Cu_2Se and the carbon. We, therefore, proposed a universal chemical principle that allows for carbon-based enhancement of Cu_2Se using a broad spectrum of carbon mesoscopic and nanoscale structures. In parallel work, Nunna et al. independently investigated carbon-nanotubes (CNTS) embedded in the Cu_2Se.[32,33] The latter results also indicate that the CNTs remain as a second unreacted phase and cause a reduction in the thermal conductivity that is broadly consistent with our work on carbon, graphite and fiber precursors. While the choice of carbon precursor does influence the electrical conductivity, the exact form of the carbon allotrope seems less critical for thermal conductivity, because different carbon sources yield broadly similar results. The mechanism for the reduction of the thermal conductivity, however, remains under debate because it does not follow the weighted-phase-volume dependency expected for a classical macro-composite. Instead, the thermal conductivity of the composite is lower than either of the constituent materials.

There are two viable mechanisms to explain the drastic reduction of the thermal conductivity in composites containing the embedded carbon structures: interfacial phonon scattering at the phase boundary of various phases, or a strong modification of the primary Cu_2Se matrix caused by, for example, atomic-scale point defects in the form of dopants. Our previous work reported calculations of the thermal boundary resistance which indicated that strong phonon reflection is expected at the interface of a graphite-like phase and Cu_2Se. Nunna et al. showed that the average speed of sound was reduced in CNT incorporated Cu_2Se, also indicating modified phonon propagation. To date, however, there has been little direct experimental information concerning the second possible mechanism: namely that the Cu_2Se crystal lattice itself is strongly modified, either by chemical reactions with carbon, the presence of carbon inclusion or by a high level of strain. In particular, the anomalous electrical conductivity and a shift in the Cu_2Se cubic-monoclinic phase transition suggest that some degree of matrix-modification does occur within the Cu_2Se. Aside from the influence on thermal and electrical conductivity, the possible formation of carbon defect structures, and the mutual solubility of C and Cu_2Se is critical because this may influence the long-term chemical stability of the C:Cu_2Se microstructure. More research is therefore needed to identify the optimal form of carbon allotrope precursors to minimize detrimental effects.

To the best of our knowledge, there have been no prior reports of the incorporation of *graphene* into a Cu_2Se matrix until now. The high surface area of the 2D carbon allotrope, however, is attractive for the purpose of enhancing surface-based chemical reactions and maximizing interfacial phonon interactions. The robust level of electronic conductivity in graphene should also be advantageous. The structural flexibility of single or multilayered graphene structures and their relative chemical stability make them ideal candidates for forming nano-inclusions in a Cu_2Se hybrid system.[34] More broadly, graphene has been found to be beneficial as an additive in other thermoelectric materials including direct doping in *n*-type and *p*-type Bi_2Te_3,[35] graphene-modified grain-boundary complexions in the Sb-based skutterudites[26] or by forming core-shell structures in nanocomposite in Fe_2P.[36]

In this article, we report a readily scalable method for incorporating of graphene nanoplates into a Cu_2Se matrix based on intense ball milling followed by melting-solidification. Using a combination of techniques including high-resolution X-ray diffraction (XRD) and scanning transmission electron microscopy (STEM) imaging, we resolve the structure at the local and global scale. Significant reduction of the thermal conductivity – from ~0.8 $W.m^{-1}.K^{-1}$ to ~0.4 $W.m^{-1}.K^{-1}$ was obtained, thus leading to a colossal thermoelectric figure-of-merit (at least zT~2.44 at 873 K at the 95% confidence level) with excellent cycling stability. Simultaneously, we noted some decrease in the electrical conductivity. However, the power factor remained comparable with the initial value owing to the enhanced Hall carrier concentration. To rationalize the results, we performed *ab initio* calculations to study each component in the composite: the Cu_2Se, the carbon Cu_2Se solid solution, graphene and graphite. The high formation energy of the solid solution was confirmed, implying that the secondary graphite and multilayer graphene phases are chemically stable. Neutron spectroscopy and *ab initio* molecular dynamics demonstrate that such carbon secondary phases are ideal phonon-scatters for Cu_2Se based on the mismatch in phonon density of states.

2. Experimental Section

2.1 Sample preparation:

Copper selenide (nominally Cu_2Se, ~99.999%) in the form of a coarse powder was obtained from Kaiyada Corp., China. The graphene nanoplatelets, having particle size and specific

surface area in the range of 5-10 μm and 300m^2/g respectively, were acquired from Sigma Aldrich, Australia (CAS: 7782-42-5). The mixtures of Cu_2Se/*x* wt% graphene nanoplatelets (*x*=0, 0.05, 0.10, 0.15, 0.30, 0.45) powder were weighed out, and sealed in a PTFE jar inside a glove box. Zirconia balls were used as milling media with a ball/material weight ratio of 10:1. Mechanical alloying was conducted by rotating the vial at 450 rpm for 5 h using a planetary ball mill. The prepared powder was then sealed in evacuated quartz ampoules and shaken above an acetylene-oxygen flame for 10 min to fully melt the powder sample without any second phase aggregation, then quickly quenched in liquid nitrogen. The as-prepared sample was then annealed in an argon atmosphere at 600 °C for recrystallization and elimination of stresses. Highly dense ingots with minimal anisotropy were obtained for all samples.

2.2 Characterization:

The phase purity of all Cu_2Se/*x* wt% graphene nanoplatelet hybrid materials was characterized by using X-ray diffraction (GBC MMA) with Cu K_α radiation within the 2θ range from 10° to 60°, followed by Rietveld refinements using the Fullprof _Suite _Windows (2017 Version). High-quality synchrotron X-ray powder diffraction was conducted at the Australian Synchrotron at a wavelength of 0.58973 Å. Silica capillaries and a Eurotherm hot air blower was used. Field emission scanning electron microscopy (FE-SEM, JEOL 7500) was used to reveal the phase composition and microstructure of as-synthesized bulk samples. Thin foils for STEM were prepared using Focused Ion Beam (FIB) milling (FEI Helios G3). STEM imaging and electron energy loss spectroscopy (EELS) were carried out on a JEOL ARM200F instrument operating at 200 kV. The Hall carrier concentration (p) was measured by a 14 T Physical Property Measurement System (Quantum Design,USA) and the correlated mobility (μ) was calculated by formula: $\sigma = pe\mu$. The electrical conductivity and Seebeck coefficient were measured simultaneously in a Argon atmosphere in the temperature range from 300 to 973 K using a RZ2001i system (Netzsch, Japan). The specific heat (*Cp*) was determined by differential scanning calorimetry on a DSC-204F1 Phoenix (Netzsh, Japan) under an Argon atmosphere with a flow rate of 50 ml/min. The sample density (ρ) was calculated using the measured weight and dimensions, and for some samples, ρ was also determined by the Archimedes method. The thermal conductivity (κ) was calculated by $\kappa = C_p \times D \times \rho$.

2.3 Neutron spectroscopy

Inelastic neutron scattering (INS) experiments were conducted on the time-of-fight cold neutron spectrometer, Pelican, at the Australian Nuclear Science and Technology

Organization. The powder samples were placed in an annular aluminum can, which was attached to the cold head of a top-loaded, closed-cycle refrigerator capable of achieving sample temperatures from 1.5 K to 700 K. The wavelength of the incident neutrons was 4.75 Å, corresponding to an energy of 3.63 meV. The Large Array Manipulation Program (LAMP) was used to reduce the data and convert the time-of-flight data to $S(Q,\omega)$, the scattering function which contains the dynamic information on the system. Background subtraction of the empty sample can and normalization to a vanadium sample , used as the isotropic scatterer, for correcting detector efficiency were also carried out. Finally, the scattering function was converted to the generalized phonon density of states (GDOS) as a function of energy transfer at the neutron-energy-gain-side. The GDOS accounts for the temperature dependence of the $S(Q,\omega)$, which is related to the thermal population of excitations.

2.4 Density functional theory calculations:

Density Functional Theory (DFT) calculations were carried out using the plane-wave code, Vienna Ab-initio Simulation Package (VASP). Geometry optimisation and molecular-dynamics (MD) simulations were performed using the Projector Augmented Wave (PAW) potential and the Perdew –Burke –Ernzerhof (PBE) exchange-correlation functional. The MD simulations used a single *k*-point at the Γ position of reciprocal space. A $(2 \times 1 \times 2)$ super-cell was used containing 97 atoms that were initially placed randomly at the 32f and 8c positions to construct disordered supercells matching the experimental occupations (see Fig. 1b) taken from previously-reported crystallographic data. Geometry optimisation and unit-cell optimisations were achieved by allowing the atoms to relax to their minimum energy positions, as reported previously. Atomic positions were all considered to be completely free, with no symmetry constraints (i.e., in the P1 space group). In the subsequent MD calculations, a time step of 1 fs was used with an energy cut-off and electronic convergence of 400 eV and 1.0×10^{-4} eV respectively. A 3 picosecond equilibration on the energy-minimized structure in the isokinetic ensemble at the target temperature was performed to distribute the kinetic energy throughout the system, followed by a 20 picosecond production run at 500 K and 675 K.

3. Results and discussions

In order to assess the structure and chemical stability of the grapheneincorporated Cu_2Se, synchrotron powder X-ray diffraction was conducted from 300–773 K (Fig. 1a). The crystal

structure of the composite sample can be indexed against the published structures for the pure monoclinic (labelled α-phase) and the cubic phase (labelled the β-phase) taken from published crystallographic data [ICSD #41140] as shown by inset in Fig. 1a. (further refinements are presented in the Supplemental Information in Figure S1). At room temperature, all composite samples exist in the low-symmetry α-phase with space group *C2/c*, indicating that the C incorporation preserves the crystal structure of the main Cu_2Se phase. The peak widths of all melt-quenched samples are considerably broadened relative to the instrument resolution, and the scattering-angle-dependency indicates both small grain sizes and strain play a role. Using Williamson-Hall analysis, the average grain-size is estimated as ~ 300 nm in the pristine material.

To gain insight into the structural behavior of the grapheneincorporated Cu_2Se under high operating temperatures, we have focused on the behavior in the regime above 400 K. Upon increasing the temperature, the Cincorporated α-Cu_2Se transforms to β-Cu_2Se with space group $Fm\bar{3}m$ (Fig. 1a), which sets in above 400 K and persists to above 773 K, in agreement with the standard Cu-Se binary phase diagram.[37] This indicates, like room temperature, the high-temperature crystal structure of the Cu_2Se is not drastically distorted by the presence of the carbon. Rietveld refinement for the cubic phase of Cu_2Se is shown in the supplemental information (Fig. S2). Fig. 1b presents an enlarged region of XRD patterns for composite samples at several temperatures. To compare the effect of heating on the microstructure, the room temperature data is compared before and after the heating cycle as shown in Fig. 1b by the dotted lines. The graphene-incorporated Cu_2Se sample undergoes no major changes after heating, whereas the pristine sample shows evidence of recrystallization at about 350 °C (Fig. S3). The microstructure of the composite sample is therefore relatively stable.

From refinement of the high-temperature powder X-ray diffraction patterns, the graphene-incorporated Cu_2Se is found to exhibit a different lattice constant and a different thermal expansion behavior (Fig. 1c). The cubic lattice parameter, *a*, is 5.805 ± 0.005 Å for the β-phase at 150 °C for the pristine sample, however, it is 5.857 ± 0.005 Å for the β-phase grapheneincorporated sample at the same temperature. The latter value matches past reports for pristine stoichiometric Cu_2Se,[38] whereas the reduced lattice constant in the carbon-free sample may arise from a small amount of Cu-deficiency forming $Cu_{2-x}Se$ in the melt-quench process. A modified lattice constant expansion is observed for the graphene/Cu_2Secomposite (Fig. 1c). The C:Cu_2Se composite displays a standard linear thermal expansion of the lattice

constant which indicates that no major chemical reactions occur in this temperature range. The pure Cu_2Se shows a clear anomaly in the lattice constant between 500 K and 600 K as shown in Fig. 1c. Similar features have been observed in past X-ray diffraction studies of pristine Cu_2Se, which assigned this feature to the change in Cu stoichiometry in this temperature interval, leading to a Cu deficiency of several percents.[38] Chemical reactions, for example, oxidation, also introduce lattice anomalies in Cu_2Se. It is noteworthy that no such features appear in carbon-containing Cu_2Se, indicating a high level of chemical stability. The diffraction patterns for the composite samples also do not display any obvious secondary phases, however, the close match of *d*-spacing in several directions (Fig. 1b) means there is considerable potential for a coherent interface with the graphite basal plane. Unfortunately, the small amount of carbon, and its low scattering power make such features difficult to detect with XRD.

Using electron microscopy, a clear two-component microstructure was observed in the grapheneincorporated Cu_2Se consisting of the primary Cu_2Se phase and secondary honeycomb carbon structures. Fig. 2a shows the microscale elemental map obtained by energy dispersive X-ray spectroscopy (EDS) via scanning electron microscopy (SEM) indicating that the Cu_2Se/graphene is solidified into a polycrystalline bulk comprised of small Cu_2Se grains with embedded carbon inclusions at spatial scales up to several micrometers. Fig. S4 shows the elemental map at higher resolution, indicating that many smaller carbon regions are also present with dimensions down to a few nanometers. STEM and TEM provide evidence of a fine grain structure, as shown in Fig. 2b-d. We can conclude that small grains of Cu_2Se are reinforced by a dense framework of intergranular carbon. Carbon inclusions can be located at grain boundaries as shown in Fig. 2e. Thin sheets of graphite or multilayered-graphene can be identified inside the matrix, generally deformed around surrounding grains as shown in Fig. 2f. An atomic-resolution image of the interface between the carbon phase and the Cu_2Se is shown in Fig. 2g in the STEM BF image. The densely packed lattice planes of the Cu_2Se lie parallel to the original graphite layered, suggesting that the phase nucleated and grew on the carbon surface. This is consistent with previous observations of carbon/Cu_2Se composites and is a feature of the crystallographic compatibility of the two phases based on the carbon honeycomb structural motif.[32,33] Fig. 2g indicates that considerable lattice expansion is also evident for Cu_2Se matrix planes near the interface as the result of epitaxial strain, as measurements of the *d*-spacing show a systematic increase nearer to the carbon phase. Based on the latter results, Fig. 2h is a schematic diagram proposing a mechanism for

nucleation and grain formation within the melt-quench process starting from the Cu_2Se and graphene precursors. At 1200 °C, graphene nanoplates, as well as Cu and Se atoms, can move randomly in the molten Cu_2Se. The limited solubility of carbon in the molten Cu_2Se allows the carbon precursors to remain undissolved and form aggregates, or remain as individual carbon sheets. This produces carbon inclusions with a hierarchical range of sizes, which is expected to have a strong effect on phonon transmission, and therefore heat transport. To demonstrate this directly, Fig. 2i shows the strong decrease of the thermal conductivity of the grapheneincorporated Cu_2Se relative to the carbon free sample, indicating a reduction of up to 50%. As expected, the complex microstructure of the graphene nanocomposite can be directly correlated with greatly reduced macroscopic heat transport.

Although the reduction of the thermal conductivity appears to be a robust feature, the electrical conductivity shows variable levels of minor deterioration in the grapheneincorporated Cu_2Se. The temperature dependence of the electrical conductivity (σ), Seebeck coefficient (S) and power factor (PF) for the pure Cu_2Se and the grapheneincorporated Cu_2Se samples are plotted in Fig. 3. Starting from x=0 to 0.15 wt%, the electrical conductivity decreases monotonically with the carbon weight percentage, while it increases for x > 0.15 wt% over a wide temperature range (Fig. 3a). Meanwhile, the temperature dependence of the Seebeck coefficient shows an inverse behavior relative to electrical conductivity as shown in Fig. 3b. The S parameter increases for x=0 to 0.15 wt%, then decreases for samples with higher graphene fraction. The complex, non-monotonic behavior of σ and S implies that two competing mechanisms affect the transport properties. The overall power factor for the composite samples are shown in Fig. 3c, and are slightly lower than the pristine sample, with the maximum PF for the composite sample reaching 10.2 $\mu W cm^{-1} K^{-2}$ at 800 K. Although graphene inclusion does lower the power factor, this is outweighed by the giant reduction in thermal conductivity and correspondingly the overall figure of merit (zT) is significantly enhanced as summarized in Fig. 3d. The carbon free sample reaches a zT of 1.1 at 873 K while the value of zT gradually increases with graphene incorporation. With graphene incorporation the zT at 873 K is increased from 1.3 for x=0.05 wt% to a maximum value of 2.44 for x=0.15 wt%, which may be the highest value of zT below 900 K among Cu_2Se based thermoelectric materials as reported. It remains as high as 2.4 to x=0.3 wt% and then drops slightly with higher fraction. These results represent considerable improvement on past results where the power factor was strongly reduced by carbon incorporation. More broadly, they also confirm the key discovery from the past

investigations: namely that the thermal conductivity can be strongly modified using a variety of carbon allotropes in the form of secondary phases embedded in the microstructure. Another crucial consideration for practical applications is the compatibility factor (s) and the related thermal mechanical properties. These are measured and reported in the Supplemental Materials (Fig. S7, 8) showing that graphene/Cu_2Se nanocomposites could be compatible with a large variety of high temperature *n*-type thermoelectric materials. While the overall performance is very promising, the anomalous non-monotonic behavior of electrical conductivity depending on the graphene fraction, and the mechanism for the reduced thermal conductivity, warrant further discussion.

In order to further clarify the effect of graphene incorporation on the electrical properties, we measured the Hall effect to determine carrier concentration (p) and mobility (μ) using $\sigma = pe\mu$. In Fig. 3e it can be seen that the p increases sharply from 6.1×10^{20} cm^{-3} for x=0, to 9.07×10^{20} cm^{-3} for x=0.05 wt%. With further incorporating, p decreases gradually down to 7.4×10^{20} cm^{-3} for x=0.45 wt%. Compared with hybrid materials comprised of carbon nanotubes and Cu_2Se, our grapheneincorporated samples show an increase in p for low levels of graphene incorporation. This suggests the possibility that the melt-quench method using high surface area graphene allows for a small amount of carbon to be alloyed with the Cu_2Se lattice. It is well established that carbon can be dissolved in liquid copper,[39] and a small amount of carbon can also be dissolved in solid copper at around 10 parts per million. No solubility data exists, however, for carbon in Cu_2Se in the liquid or solid phase.[40] Using electron-loss-spectroscopy, we were unable to detect any substantial carbon signal from the solid-state Cu_2Se matrix within the limitations of the technique (~ 0.1 wt%), indicating solubility is low.

Fig. 3f represents the temperature dependent heat capacity under constant pressure (*Cp*) of synthesized samples with different graphene concentrations. All the samples show similar *Cp* values for β-phase which is consistent with Dulong-Petit's law. While the shape and the peak position indicatea continuous phase transition of Cu_2Se which shifts to high temperatures with increasing graphene concentration.

To theoretically assess the possibility that carbon can dissolve in the Cu_2Se matrix at very low concentrations and act as a dopant, we calculated the defect formation energy using density functional theory. We modelled $2 \times 2 \times 2$ supercells containing 97 atoms arranged in the

cubic phase of Cu_2Se. This corresponds to a carbon concentration of 1.03 atomic % or 0.065 wt%. The cubic phase structure of β-Cu_2Se was used as the basis for the calculation, as it is the high-temperature properties of the C:Cu_2Se system which are the key factors during both synthesis and operation. Carbon was trialled in 6 different positions, 4 interstitials and three possible substitutional sites. For each position, 3 different disordered configurations were used for copper positions. The lowest energy defect was identified to be interstitial carbon, octahedrally coordinated with copper and forming Cu-C bonds with a length of 1.96-2.1 Å as shown in Fig. 4a. For comparison, the corresponding carbon free system with the same initial copper configuration is shown in Fig. 4b. The comparison shows that, if present, C would distorts the cubic lattice significantly in contrast to the experimental observations. The lattice expansion caused by this interstitial dopant was calculated to be in the range of 0.4 – 0.6 %. To calculate the formation energy for an interstitial carbon defect via solid-state chemical reactions, we deployed the formula:

$$E_F = E(Cu_2SeC_x) - E(Cu_2Se) - x^*E(C) \quad \ldots\ldots (1)$$

where the first term corresponds to the total energy of the carbon doped Cu_2Se supercell, the second is energy of pure Cu_2Se in the cubic phase with the same supercell dimensions, and the final term is the energy per carbon in the starting material (in this case either graphite or graphene), weighted by the number of carbon atoms in the supercell (x^*). To make a careful comparison, the same copper configuration was used when evaluating the energy of the doped and undoped phases, subject only to a small amount of ionic relaxation. Although there is some unavoidable variance in the trial configurations, the results consistently show the formation energies lie in the range +2.6 to +3.2 eV for carbon in the various interstitial sites. The formation energies for the carbon defect derived from monolayer graphene is slightly lower by 9.3 meV relative to the graphite precursors, because of the decreased van der Waals interaction. Other interstitial sites, such as the carbon within the center of the unoccupied copper cage, resulted in similar energies after ionic relaxation. The hypothetical electronic density of states for one representative defect configuration is shown in Figure S9. The key result, however, is the formation energies are prohibitively high, and in the thermodynamic limit, there would be a negligible percentage of carbon point-defects in Cu_2Se in a solid-state environment, well below parts per million.

The XRD and electron microscopy data, supported by the theoretical calculations, show that it is chemically-preferable for a majority of carbon to remain as inert graphene and graphite secondary phases in the solid state matrix of Cu_2Se. The high formation energy indicated by

DFT calculations suggest it is energetically unfavorable to form a solid solution containing carbon dissolved in Cu_2Se. Furthermore, there are no other ternary compounds containing Cu, Se and C reported in the Inorganic Crystal Structure Database (ICSD). Thus, there are few, if any, chemical reactions possible in the composite C:Cu_2Se system. This is consistent with the high-temperature X-ray diffraction because secondary phases would be detected or a much larger expansion would result if more than 0.065 wt% of carbon were reacted or dissolved. Instead, the overall microstructure is stable upon heating, indicating that carbon nano-inclusions generally survive as secondary unreacted phases and do not undergo solid-state reactions. Collectively, this explains the hierarchal distribution of carbon nanostructures sizes embedded in the Cu_2Se. The largest sizes are influenced by the degree of agglomeration of the carbon precursors during the synthesis procedure, which is generally enhanced in the liquid state of the Cu_2Se in the first stage of the synthesis. Carbon that is metastably dissolved in the liquid phase of Cu_2Se is expected to form precipitates upon cooling. The smallest size of the nanostructure ensemble will then be determined by the initial size of the carbon precursor or the precipitates, depending on synthesis conditions. A mechanistic consequence of the chemically-stable hierarchal microstructure is that the phonon scattering will be greatly modified because the resulting local vibrational density of states will be inhomogeneous across the interface of the carbon phase and Cu_2Se.

The established theories of interfacial boundary resistance and interfacial phonon scattering can yield useful insights into the high temperature phonon scattering of carbon embedded to form inhomogeneous structures in Cu_2Se.[41–44] In previous work, we deployed the acoustic mismatch model (AMM) which explains why there is a strong reflection of phonons at the C:Cu_2Se interfaces below a critical angle as illustrated schematically in Fig. 5a based on the mismatch in mass density and speed of sound of the two components. On the other hand, the model implies a strong temperature dependency, which was not observed experimentally. This is a well-known shortcoming in the AMM. A full understanding of phonon scattering at all temperatures for nanostructures embedded in thermoelectric materials remains challenging because many factors play a role: nature of interfacial bonding, the contribution of contact versus boundary resistance and role of the nanomorphology. On general grounds, however, it is clear that the high surface area of planar nanostructures, such as graphene, will provide an increased cross-section for interfacial phonon scattering. On the other hand, the degree of phonon-transparency of the individual interfaces is also a key factor. In the following section, we extend the previous work and propose a mechanism whereby interfacial phonons can be

scattered diffusely as in Fig. 5b. This results in a high thermal boundary resistance for the graphite/graphene:Cu_2Se interfaces based on the mismatch in the phonon density of states.[41]

The diffuse mismatch model (DMM)[41] was developed to explain the diffuse reflection of phonons between two dissimilar materials that occurs at high temperatures as shown schematically in Fig. 5a, where the AMM is inapplicable. In this limit of the DMM, the precise angle of the scattering becomes unimportant, as phonons are effectively randomized and lose memory of their incoming direction. Consequently, the model only depends on angle-integrated density-of-states of each material, the velocity magnitude of the incoming phonon in Material A and outgoing phonon mode in Material B. With the diffuse mismatch model, the transmission probability (α) of a phonon i with frequency ω escaping material A and entering material B can be written as:

$$\alpha_i(\omega_i) = \frac{\sum_j G_B(\omega_i,T)c_{i,B}}{\sum_j G_A(\omega_i,T)c_{i,A}} \quad \ldots\ldots (2)$$

In equation 2, $G_A(\omega_i,T)$ is phonon density of states at energy ω in material A at temperature T, and $G_B(\omega_i,T)$ is the phonon density of states at the same energy in material B. This must be summed over all j modes, both transverse and longitudinal. The velocity (dispersion) of each phonon mode is modelled by the parameter $c_{i,A}$ and $c_{i,B}$ in each material. Only modes below a maximum frequency ω_{Max} contribute to the heat flow across the interface, where the cutoff frequency is determined by the specific phonon properties of the materials.[41] At low temperatures, the Debye approximation can be used to model G_A and G_B. However, in the high-temperature limit, it is necessary to consider the true density of states and phonon dispersion, because $G_A(\omega_i,T)$ and $G_B(\omega_i,T)$ contain considerable substructure including forbidden gap regions and sharp regions with high density of states (van Hove singularities). A key implication of the model is that phonon transmission will be very poor if $G_B(\omega_i,T)$ has a low (or zero) density of states in a frequency regime where $G_A(\omega_i,T)$ has a high density of states. We now show that this is exactly the situation encountered by phonons in the grapheneincorporated Cu_2Se, and carbon-Cu_2Se composites.

To investigate the substructure of $G_A(\omega_i,T)$ and $G_B(\omega_i,T)$, and show the mismatch in the density of states, we performed neutron spectroscopy of Cu_2Se and compared this with *ab initio* molecular dynamics calculations based on density functional theory. Time-of-flight neutron spectroscopy measures the generalized density of states, proportional to the total

density of phonon states integrated over all angles, weighted by the incoherent scattering power of the individual elements, and convoluted with the resolution function of the instrument. Fig. 5b shows the generalized density of states (GDOS) measured and calculated for pure Cu_2Se, and for nanographite particles, based on our experimental data for Cu_2Se and the published data of Cavallari and Rols et al. for nanographite.[45] The experimental GDOS for the pristine Cu_2Se is in excellent agreement with other recent measurements,[46] and the graphene incorporated sample exhibits a nearly identical GDOS within the level of experimental uncertainty. In contrast, if a solid-solution were formed between C and Cu2Se, additional features from rattling modes would be expected according to ab initio molecular dynamics (Fig. S10), however these are not observed experimentally.

A characteristic feature in the Cu_2Se neutron data, evident for composite samples, is that the majority of phonon modes are present below 40 meV. The broad spectral feature is the superposition of a large number of phonon modes, including acoustic phonon modes with very short life time and correspondingly, large phonon line widths in the range 3-15 meV[18,47] and short mean free path. Superimposed in Fig. 5 is the Cartesian vibrational density of states calculated by Fourier transforming the molecular dynamics trajectory using techniques discussed in past work.[48,49] The agreement between the main spectral features in the theoretical density of states and experimental density of states is excellent for Cu_2Se, and main low energy features are well reproduced. In comparison, the graphite, in bulk or in nanostructure form[45] has a more classical continuous distribution of phonon modes extending far above 40 meV, with a few well-defined regions with high density of states (van Hove Singularities) near phonon band minima or maxima distributed between 0 – 100 meV. The vibrational density of states calculated with the DFT method for graphite predicts the position of the main van Hove singularities in agreement with past results,[45] although the continuum of long wavelength acoustic phonons is not fully reproduced owing to the small simulation size. For the purposes here, the important result shown both in the theory and the experiment is that the regions of high density of states in Cu_2Se, which can be labelled $G_A(\omega_i, T)$ below 40 meV overlap regions of low density of states in graphite $G_B(\omega_i, T)$, leading to strong phonon scattering at their mutual interface according to Equation 2. A coarse estimate using the density of states from the molecular dynamics, and assuming a constant speed of sound ratio c_g/c_{Cu_2Se} = 7.3 for the phonon modes based on the relative average speed of sound, indicates that phonon transmission will be very low (10-20%) for a wide range of phonon energies below 40 meV. Furthermore, above ω_{Max} ~ 40 meV as defined by

the fall-off in the Cu_2Se spectrum, there will be minimal contribution to heat-flow because there almost no available modes in the Cu_2Se, making heat transmission via phonons forbidden at the level of a first-order single phonon processes. Broadly similar arguments hold for wide variety of carbon allotropes based on the structural honeycomb motif, including graphene, because all these exhibit a wide distribution of phonon energies unlike Cu_2Se. Finally, as the density of states of Cu_2Se does not exhibit a strong temperature dependency between 300 - 900 K,[18] the interfacial boundary resistance from diffuse phonon scattering will be strong in the entire temperature range.

4. Conclusion

We used intense ball milling followed by the melt-quench process to fabricate a nanocomposite material consisting of graphene nanoplatelets incorporated into a Cu_2Se matrix. The as-prepared sample with 0.15 wt% graphene showed a significant reduction of thermal conductivity from ~0.8 $W \cdot m^{-1} \cdot K^{-1}$ to ~0.4 $W \cdot m^{-1} \cdot K^{-1}$, leading to a very high thermoelectric figure-of-merit (zT~2.44 at 873 K) with reliable cycling stability. The temperature dependency of the other thermoelectric relevant parameters (σ, S, PF, etc.) was also measured systematically from 300 K to 873 K and the results showed a correlation with the graphene content. Electron microscopy revealed a hierarchal composite microstructure consisting of nanoscale Cu_2Se grains enclosed within a carbonaceous network. The presence of the carbonaceous material at the grain boundaries reduces both thermal and electrical conductivity, but the effect on thermal conductivity is greater, leading to a significant enhancement of zT. Synchrotron X-ray powder diffraction results demonstrate a moderate degree of lattice expansion of graphene incorporated samples compared with pristine Cu_2Se and showed that no solid-state reactions between carbon and Cu_2Se occurred up to high temperatures. This is rationalized using density functional theory calculations which show that the solid-solution of carbon in Cu_2Se is enthalpically unfavorable. The novel liquid phase mixing employed in the synthesis of these materials leads to a hierarchal microstructure consisting of carbon inclusions at various spatial scales. The mechanism for the reduced heat transport is correlated with the phonon density of states of multi-layered graphene or graphite and Cu_2Se which are poorly matched. This is the key to inhibiting phonon transport across the inhomogeneous microstructure. The reduction in thermal conductivity has an important effect on enhancing the zT of C/Cu_2Se composites. A full quantitative treatment of the thermal conductivity, possibly using the diffuse mismatch model to assess the upper limits on the

thermoelectric performance, would be very useful, but this demands new numerical techniques involving the full dispersion and velocity of each phonon branch which is beyond the scope of this work. Nevertheless, if the underlying model is correct, then incorporating chemically-stable low-atomic-mass materials with a mismatch in their phonon density of states into hierarchal microstructures containing a heavy thermoelectric matrix will be a generally effective strategy to enhance thermoelectric performance.

Acknowledgements

This work was partially supported by the Australian Research Council (ARC) through a Discovery Project DP 130102956 (XLW), an ARC Professorial Future Fellowship project (FT 130100778, XLW) and a Linkage Infrastructure Equipment and Facilities (LIEF) Grant (LE 120100069, XLW). We acknowledge the fruitful discussions with Dr. Robert Robinson. We thank the Australian Synchrotron and ANSTO for access to X-ray and neutron instruments. Dr. Mitchell Nancarrow of the UOW EMC is thanked for assistance with sample preparation and SEM analysis. This research used equipment (FIB and STEM) funded by the ARC LIEF grants: LE160100063 and LE120100104 respectively, located at the UOW Electron Microscopy Centre.

Supporting Information

Supplementary data associated with this article can be found in the online version.

References

[1] C. Chang, M. Wu, D. He, Y. Pei, C.-F. Wu, X. Wu, H. Yu, F. Zhu, K. Wang, Y. Chen, L. Huang, J.-F. Li, J. He, L.-D. Zhao, 3D charge and 2D phonon transports leading to high out-of-plane ZT in n-type SnSe crystals, Science (80-.). 360 (2018) 778 LP-783. http://science.sciencemag.org/content/360/6390/778.abstract.

[2] Y. Yang, K.C. Pradel, Q. Jing, J.M. Wu, F. Zhang, Y. Zhou, Y. Zhang, Z.L. Wang, Thermoelectric Nanogenerators Based on Single Sb-Doped ZnO Micro/Nanobelts, ACS Nano. 6 (2012) 6984–6989. doi:10.1021/nn302481p.

[3] Y. Yang, W. Guo, K.C. Pradel, G. Zhu, Y. Zhou, Y. Zhang, Y. Hu, L. Lin, Z.L. Wang, Pyroelectric Nanogenerators for Harvesting Thermoelectric Energy, Nano Lett. 12 (2012) 2833–2838. doi:10.1021/nl3003039.

[4] G.J. Snyder, E.S. Toberer, Complex thermoelectric materials, Nat. Mater. 7 (2008) 105. doi:10.1038/nmat2090.

[5] L.E. Bell, Cooling, Heating, Generating Power, and Recovering Waste Heat with Thermoelectric Systems, Science (80-.). 321 (2008) 1457. http://science.sciencemag.org/content/321/5895/1457.abstract.

[6] L. Yang, Z.-G. Chen, M.S. Dargusch, J. Zou, High Performance Thermoelectric Materials: Progress and Their Applications, Adv. Energy Mater. (n.d.) 1701797–n/a. doi:10.1002/aenm.201701797.

[7] J. He, T.M. Tritt, Advances in thermoelectric materials research: Looking back and moving forward, Science (80-.). 357 (2017). http://science.sciencemag.org/content/357/6358/eaak9997.abstract.

[8] Y. Yang, Z.-H. Lin, T. Hou, F. Zhang, Z.L. Wang, Nanowire-composite based flexible thermoelectric nanogenerators and self-powered temperature sensors, Nano Res. 5 (2012) 888–895. doi:10.1007/s12274-012-0272-8.

[9] X. Wang, Z.L. Wang, Y. Yang, Hybridized nanogenerator for simultaneously scavenging mechanical and thermal energies by electromagnetic-triboelectric-thermoelectric effects, Nano Energy. 26 (2016) 164–171. doi:https://doi.org/10.1016/j.nanoen.2016.05.032.

[10] A.J. Minnich, M.S. Dresselhaus, Z.F. Ren, G. Chen, Bulk nanostructured thermoelectric materials: current research and future prospects, Energy Environ. Sci. 2 (2009) 466–479. doi:10.1039/B822664B.

[11] T. Zhu, Y. Liu, C. Fu, J.P. Heremans, J.G. Snyder, X. Zhao, Compromise and Synergy in High-Efficiency Thermoelectric Materials, Adv. Mater. 29 (2017) 1605884–n/a. doi:10.1002/adma.201605884.

[12] L.S.S. A. F. Ioffe E. K. Iordanishvili, T. S. Stavitskaya, A. Gelbtuch, Semiconductor Thermoelements and Thermoelectric Cooling, Phys. Today. 12 (1959) 42.

[13] T.M. Tritt, M.A. Subramanian, Thermoelectric Materials, Phenomena, and Applications: A Bird's Eye View, MRS Bull. 31 (2006) 188–198. doi:10.1557/mrs2006.44.

[14] J. Shuai, H. Geng, Y. Lan, Z. Zhu, C. Wang, Z. Liu, J. Bao, C.-W. Chu, J. Sui, Z. Ren, Higher thermoelectric performance of Zintl phases (Eu0.5Yb0.5)1−xCaxMg2Bi2 by band engineering and strain fluctuation, Proc. Natl. Acad. Sci. 113 (2016) E4125–E4132. doi:10.1073/pnas.1608794113.

[15] T.M. Tritt, Thermoelectric Phenomena, Materials, and Applications, Annu. Rev. Mater. Res. 41 (2011) 433–448. doi:10.1146/annurev-matsci-062910-100453.

[16] H. Liu, X. Shi, F. Xu, L. Zhang, W. Zhang, L. Chen, Q. Li, C. Uher, T. Day, G.J. Snyder, Copper ion liquid-like thermoelectrics, Nat. Mater. 11 (2012) 422. doi:10.1038/nmat3273https://www.nature.com/articles/nmat3273#supplementary-information.

[17] X. Su, F. Fu, Y. Yan, G. Zheng, T. Liang, Q. Zhang, X. Cheng, D. Yang, H. Chi, X. Tang, Q.

Zhang, C. Uher, Self-propagating high-temperature synthesis for compound thermoelectrics and new criterion for combustion processing, Nat. Commun. 5 (2014) 4908. doi:10.1038/ncomms5908https://www.nature.com/articles/ncomms5908#supplementary-information.

[18] D.J. Voneshen, H.C. Walker, K. Refson, J.P. Goff, Hopping Time Scales and the Phonon-Liquid Electron-Crystal Picture in Thermoelectric Copper Selenide, Phys. Rev. Lett. 118 (2017) 145901. https://link.aps.org/doi/10.1103/PhysRevLett.118.145901.

[19] X.S. Pengfei Qiu Lidong Chen, Materials Aspect of Thermoelectricity, CRC Press, 2016.

[20] P. Peng, Z.N. Gong, F.S. Liu, M.J. Huang, W.Q. Ao, Y. Li, J.Q. Li, Structure and thermoelectric performance of β-Cu2Se doped with Fe, Ni, Mn, In, Zn or Sm, Intermetallics. 75 (2016) 72–78. doi:https://doi.org/10.1016/j.intermet.2016.05.012.

[21] T.W. Day, K.A. Borup, T. Zhang, F. Drymiotis, D.R. Brown, X. Shi, L. Chen, B.B. Iversen, G.J. Snyder, High-temperature thermoelectric properties of Cu1.97Ag0.03Se1+y, Mater. Renew. Sustain. Energy. 3 (2014) 26. doi:10.1007/s40243-014-0026-5.

[22] S.D. Kang, J.-H. Pöhls, U. Aydemir, P. Qiu, C.C. Stoumpos, R. Hanus, M.A. White, X. Shi, L. Chen, M.G. Kanatzidis, G.J. Snyder, Enhanced stability and thermoelectric figure-of-merit in copper selenide by lithium doping, Mater. Today Phys. 1 (2017) 7–13. doi:https://doi.org/10.1016/j.mtphys.2017.04.002.

[23] H. Liu, X. Yuan, P. Lu, X. Shi, F. Xu, Y. He, Y. Tang, S. Bai, W. Zhang, L. Chen, Y. Lin, L. Shi, H. Lin, X. Gao, X. Zhang, H. Chi, C. Uher, Ultrahigh Thermoelectric Performance by Electron and Phonon Critical Scattering in Cu2Se1-xIx, Adv. Mater. 25 (2013) 6607–6612. doi:10.1002/adma.201302660.

[24] L. Zhao, F.Y. Fei, J. Wang, F. Wang, C. Wang, J. Li, J. Wang, Z. Cheng, S. Dou, X. Wang, Improvement of thermoelectric properties and their correlations with electron effective mass in Cu(1.98)S(x)Se(1−x), Sci. Rep. 7 (2017) 40436. doi:10.1038/srep40436.

[25] L. Yang, Z.-G. Chen, G. Han, M. Hong, L. Huang, J. Zou, Te-Doped Cu2Se nanoplates with a high average thermoelectric figure of merit, J. Mater. Chem. A. 4 (2016) 9213–9219. doi:10.1039/C6TA02998A.

[26] P. Zong, R. Hanus, M. Dylla, Y. Tang, J. Liao, Q. Zhang, G.J. Snyder, L. Chen, Skutterudite with graphene-modified grain-boundary complexion enhances zT enabling high-efficiency thermoelectric device, Energy Environ. Sci. 10 (2017) 183–191. doi:10.1039/C6EE02467J.

[27] Y. He, P. Lu, X. Shi, F. Xu, T. Zhang, G.J. Snyder, C. Uher, L. Chen, Ultrahigh Thermoelectric Performance in Mosaic Crystals, Adv. Mater. 27 (2015) 3639–3644. doi:10.1002/adma.201501030.

[28] R. Liu, H. Chen, K. Zhao, Y. Qin, B. Jiang, T. Zhang, G. Sha, X. Shi, C. Uher, W. Zhang, L. Chen, Entropy as a Gene-Like Performance Indicator Promoting Thermoelectric Materials, Adv. Mater. 29 (2017) 1702712–n/a. doi:10.1002/adma.201702712.

[29] Y.Y. Li, X.Y. Qin, D. Li, J. Zhang, C. Li, Y.F. Liu, C.J. Song, H.X. Xin, H.F. Guo, Enhanced thermoelectric performance of Cu2Se/Bi0.4Sb1.6Te3 nanocomposites at elevated temperatures, Appl. Phys. Lett. 108 (2016) 62104. doi:10.1063/1.4941757.

[30] K. Biswas, J. He, I.D. Blum, C.-I. Wu, T.P. Hogan, D.N. Seidman, V.P. Dravid, M.G. Kanatzidis, High-performance bulk thermoelectrics with all-scale hierarchical architectures, Nature. 489 (2012) 414. doi:10.1038/nature11439https://www.nature.com/articles/nature11439#supplementary-information.

[31] L.-D. Zhao, S. Hao, S.-H. Lo, C.-I. Wu, X. Zhou, Y. Lee, H. Li, K. Biswas, T.P. Hogan, C. Uher, C. Wolverton, V.P. Dravid, M.G. Kanatzidis, High Thermoelectric Performance via Hierarchical Compositionally Alloyed Nanostructures, J. Am. Chem. Soc. 135 (2013) 7364–7370. doi:10.1021/ja403134b.

[32] L. Zhao, S.M.K.N. Islam, J. Wang, D.L. Cortie, X. Wang, Z. Cheng, J. Wang, N. Ye, S. Dou, X. Shi, L. Chen, G.J. Snyder, X. Wang, Significant enhancement of figure-of-merit in carbon-reinforced Cu2Se nanocrystalline solids, Nano Energy. 41 (2017) 164–171. doi:https://doi.org/10.1016/j.nanoen.2017.09.020.

[33] R. Nunna, P. Qiu, M. Yin, H. Chen, R. Hanus, Q. Song, T. Zhang, M.-Y. Chou, M.T. Agne, J. He, G.J. Snyder, X. Shi, L. Chen, Ultrahigh thermoelectric performance in Cu2Se-based hybrid materials with highly dispersed molecular CNTs, Energy Environ. Sci. 10 (2017) 1928–1935. doi:10.1039/C7EE01737E.

[34] A.A. Balandin, Thermal properties of graphene and nanostructured carbon materials, Nat. Mater. 10 (2011) 569. doi:10.1038/nmat3064.

[35] A.A.A. Rahman, A.A. Umar, X. Chen, M.M. Salleh, M. Oyama, Enhanced thermoelectric properties of bismuth telluride–organic hybrid films via graphene doping, Appl. Phys. A. 122 (2016) 133. doi:10.1007/s00339-016-9659-9.

[36] J. Yang, Y. Ouyang, H. Zhang, H. Xu, Y. Zhang, Y. Wang, Novel Fe2P/graphitized carbon yolk/shell octahedra for high-efficiency hydrogen production and lithium storage, J. Mater. Chem. A. 4 (2016) 9923–9930. doi:10.1039/C6TA03501A.

[37] K. Stephen Dongmin, A.D. Sergey, A. Umut, A. Maxim, S. Andrew, G.J. Snyder, Apparent critical phenomena in the superionic phase transition of Cu 2- x Se, New J. Phys. 18 (2016) 13024. http://stacks.iop.org/1367-2630/18/i=1/a=013024.

[38] A.N. Skomorokhov, D.M. Trots, M. Knapp, N.N. Bickulova, H. Fuess, Structural behaviour of β-Cu2−δSe (δ=0, 0.15, 0.25) in dependence on temperature studied by synchrotron powder diffraction, J. Alloys Compd. 421 (2006) 64–71. doi:https://doi.org/10.1016/j.jallcom.2005.10.079.

[39] S. Amini, J. Garay, G. Liu, A.A. Balandin, R. Abbaschian, Growth of large-area graphene films from metal-carbon melts, J. Appl. Phys. 108 (2010) 94321. doi:10.1063/1.3498815.

[40] S. Saji, T. Kadokura, H. Anada, K. Notoya, N. Takano, Solid Solubility of Carbon in Copper during Mechanical Alloying, Mater. Trans. JIM. 39 (1998) 778–781. doi:10.2320/matertrans1989.39.778.

[41] E.T. Swartz, R.O. Pohl, Thermal boundary resistance, Rev. Mod. Phys. 61 (1989) 605–668. https://link.aps.org/doi/10.1103/RevModPhys.61.605.

[42] D.G. Cahill, W.K. Ford, K.E. Goodson, G.D. Mahan, A. Majumdar, H.J. Maris, R. Merlin, S.R. Phillpot, Nanoscale thermal transport, J. Appl. Phys. 93 (2002) 793–818. doi:10.1063/1.1524305.

[43] Y. Benveniste, T. Miloh, The effective conductivity of composites with imperfect thermal contact at constituent interfaces, Int. J. Eng. Sci. 24 (1986) 1537–1552. doi:https://doi.org/10.1016/0020-7225(86)90162-X.

[44] Y. Benveniste, Effective thermal conductivity of composites with a thermal contact resistance between the constituents: Nondilute case, J. Appl. Phys. 61 (1987) 2840–2843. doi:10.1063/1.337877.

[45] C. Cavallari, D Pontiroli, M. Jiménez-Ruiz, A. Ivanov, M. Mazzani, M. Gaboardi, M. Aramini, M. Brunelli, M. Riccò, S. Rols, Hydrogen on graphene investigated by inelasticneutron scattering, J. Phys. Conf. Ser. 554 (2014) 12009.

[46] H. Liu, J. Yang, X. Shi, S.A. Danilkin, D. Yu, C. Wang, W. Zhang, L. Chen, Reduction of thermal conductivity by low energy multi-Einstein optic modes, J. Mater. 2 (2016) 187–195. doi:https://doi.org/10.1016/j.jmat.2016.05.006.

[47] S.A. Danilkin, A.N. Skomorokhov, A. Hoser, H. Fuess, V. Rajevac, N.N. Bickulova, Crystal structure and lattice dynamics of superionic copper selenide Cu2−δSe, J. Alloys Compd. 361 (2003) 57–61. doi:https://doi.org/10.1016/S0925-8388(03)00439-0.

[48] D.L. Cortie, B.R. McBride, N. Narayanan, N.R. de Souza, M. Avdeev, R.A. Mole, G.J. McIntyre, G.J. Kearley, R. Withers, D.H. Yu, Y. Liu, Time-Disordered Crystal Structure of AlPO4-5, J. Phys. Chem. C. 121 (2017) 18762–18770. doi:10.1021/acs.jpcc.7b06415.

[49] H. Kim, S. Ballikaya, H. Chi, J.-P. Ahn, K. Ahn, C. Uher, M. Kaviany, Ultralow thermal conductivity of β-Cu2Se by atomic fluidity and structure distortion, Acta Mater. 86 (2015) 247–253. doi:https://doi.org/10.1016/j.actamat.2014.12.008.

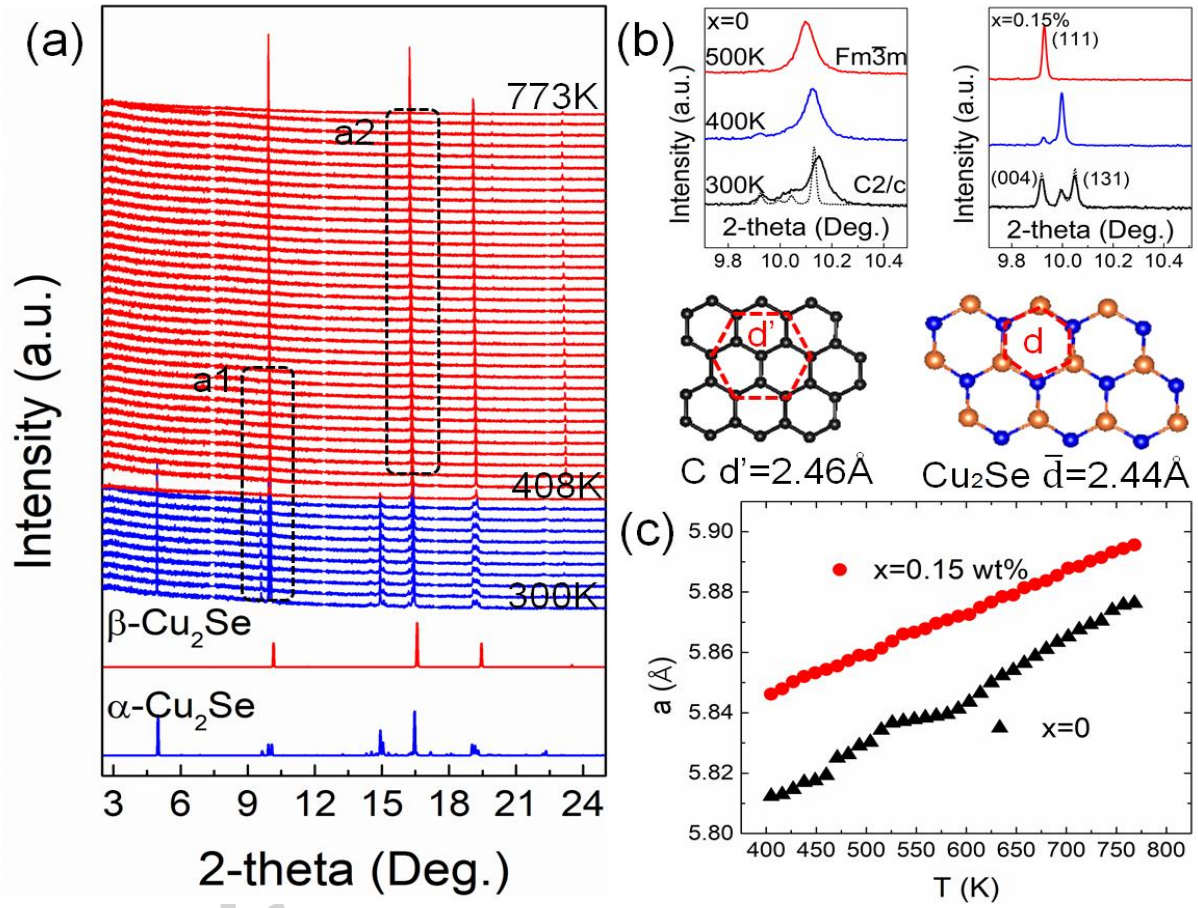

Figure 1. (a) Synchrotron powder diffraction patterns of Cu_2Se / 0.15 wt% graphene nanoplatelets sample heated from room temperature (RT) to 773 K, simulated powder diffraction patterns for *α*-Cu_2Se and *β*-Cu_2Se are also presented at the bottom of the figure. (b) (top) Enlarged diffraction patterns for regions a1 (Fig. 1a) for the pristine and composite sample at selected temperatures. The dotted line shows the patterns following the heating process after returning to 300 K. (bottom) Schematic diagram of graphene and Cu_2Se crystal lattice seen from <010> and <001> directions, respectively. (c) Temperature dependence of the lattice parameter of pristine and composite samples (*x*=carbon fraction (wt%)) in the range marked as a2.

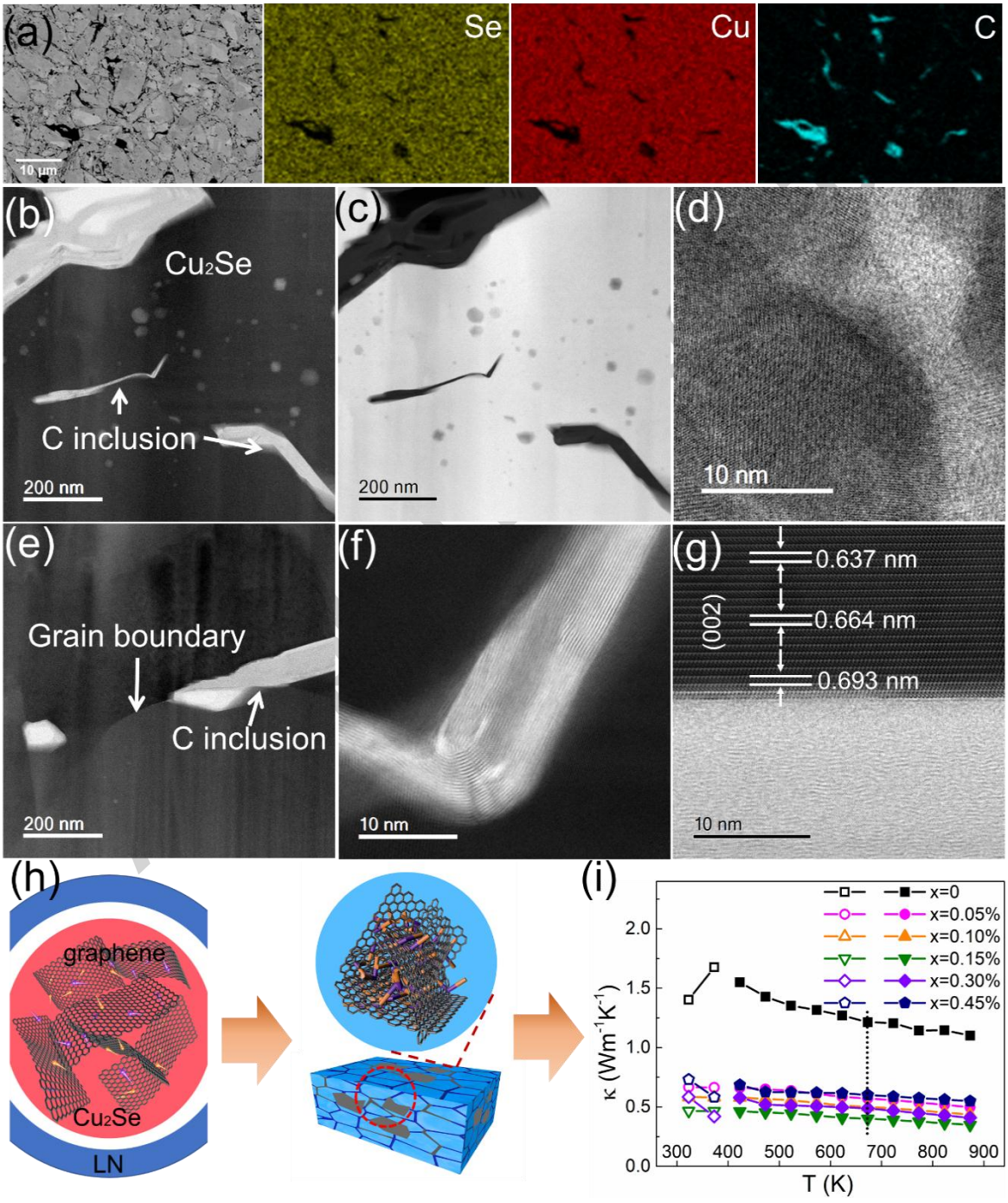
(a)
10 μm
Se
Cu
C
(b)
Cu2Se
C inclusion
200 nm
(c)
200 nm
(d)
10 nm
(e)
Grain boundary
C inclusion
200 nm
(f)
10 nm
(g)
0.637 nm
0.664 nm
0.693 nm
(002)
10 nm
(h)
graphene
Cu2Se
LN
(i)
x=0
x=0.05%
x=0.10%
x=0.15%
x=0.30%
x=0.45%
κ (Wm-1K-1)
T (K)

Figure 2. (a) SEM backscattered image and associated EDS maps for ion beam polished Cu_2Se/0.45 wt% GNPs. STEM (b) BF and (c) HAADF images showing the presence dispersion of large angular carbon inclusions and smaller rounded voids. (d) HRTEM image showing the allocation of nano-sized sublattice. (e) STEM BF image of graphitic inclusions lying on a Cu_2Se grain boundary. (f) STEM BF image of a multi-layered graphene particle embedded in the Cu_2Se matrix (dark). (g) STEM BF image of the interface where Cu_2Se nucleated on the graphitic carbon (bottom) triggering enlargement of lattice constant near the interface. (h) Schematic diagram of the nucleation process leading to small grains. (i) Ultralow thermal conductivity achieved by graphene nanoplatelets incorporation.

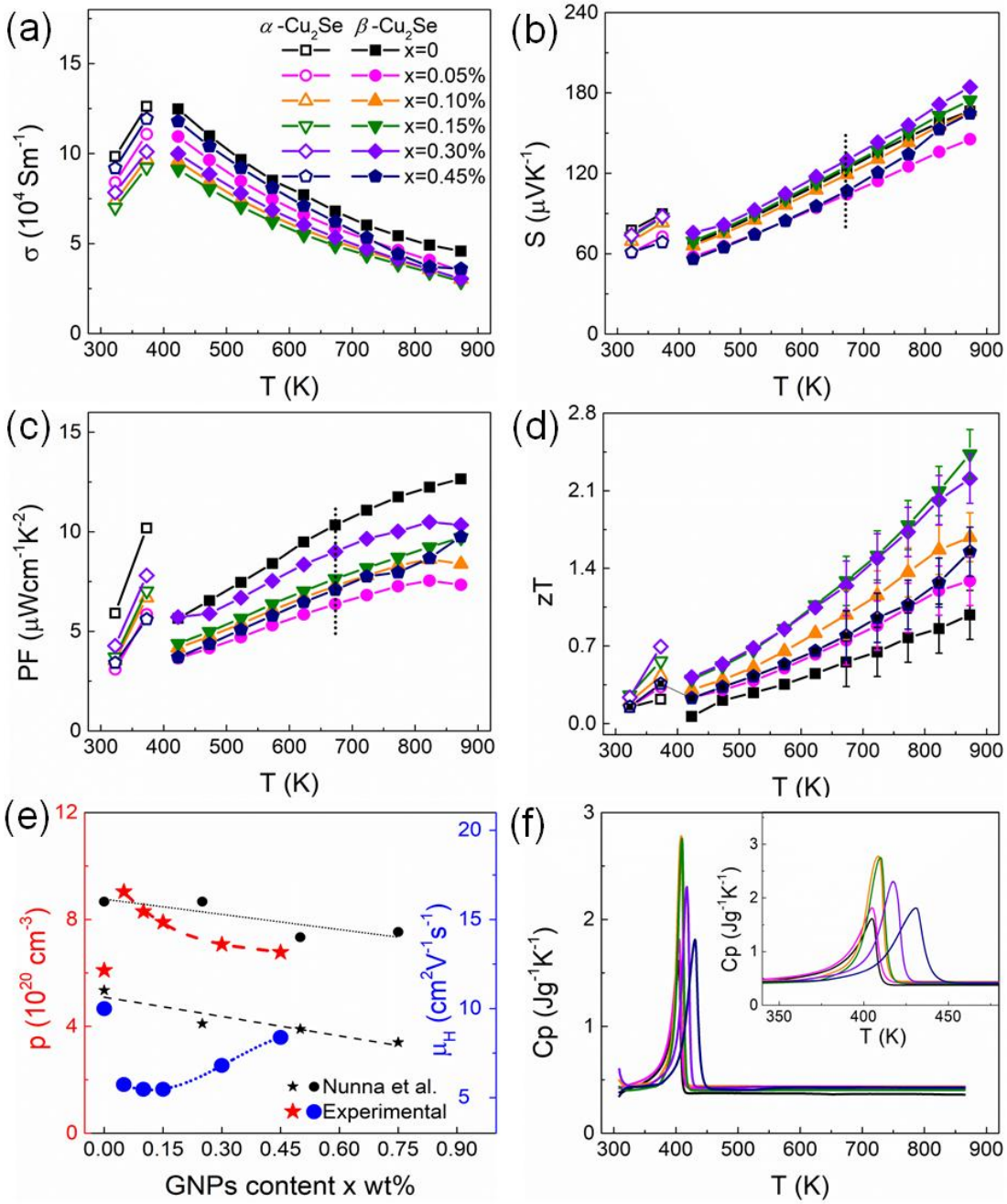

Figure 3. Temperature dependence of thermoelectric electrical properties of pristine and composite Cu_2Se samples: (a) electrical conductivity (σ), (b) Seebeck coefficient (S), (c) power factor (PF), (d) zT, (e) Hall hole concentration and Hall mobility as a function of the content of GNPs at 300 K. The data for the Cu_2Se /carbon nanotubes hybrid materials reported in ref. 15b is also included for comparison. (The empty symbols refer to the results before phase transition) (e) Specific heat capacity at constant pressure (C_p) of samples with different graphene fraction, inset is the C_p results during phase transition.

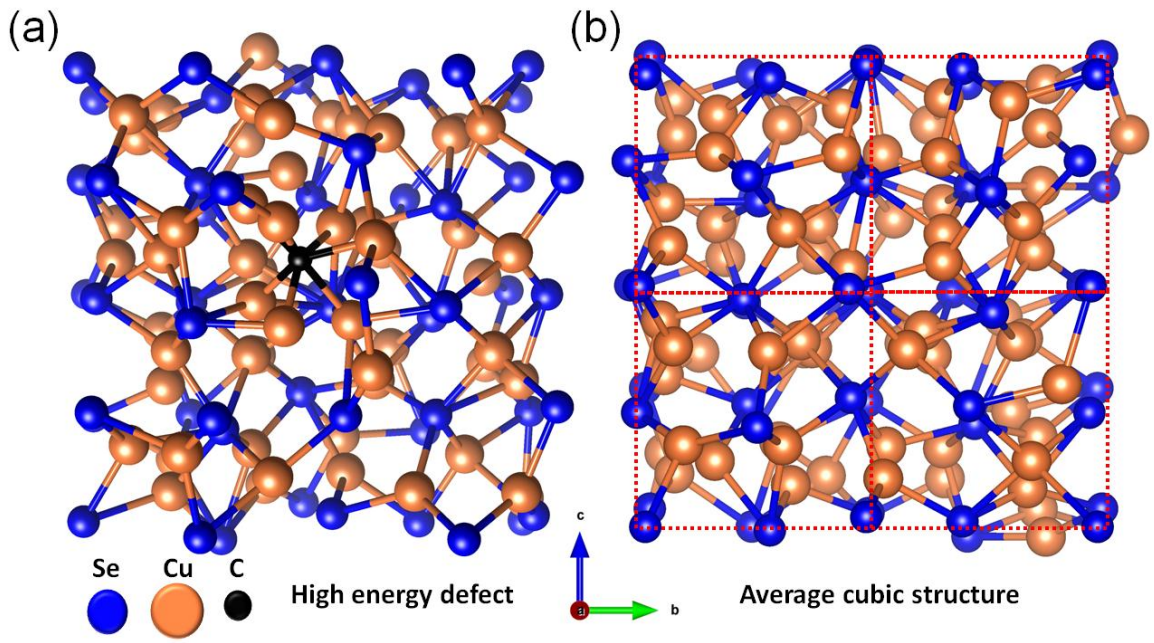

Figure 4. (a) Theoretical configuration of an interstitial carbon defect as calculated by DFT. Although the interstitial defect is more energetically-favorable than substitutional defects, it has a high formation energy at 2.6-3.1 eV and causes a strong distortion of the lattice during ionic relaxation. (b) The identical supercell to (a) pictured without the carbon defect. The dashed lines indicate the position of the average cubic structure formed by the Se lattice, whereas the Cu occupy disordered positions in the 32f and 8c Wyckoff sites.

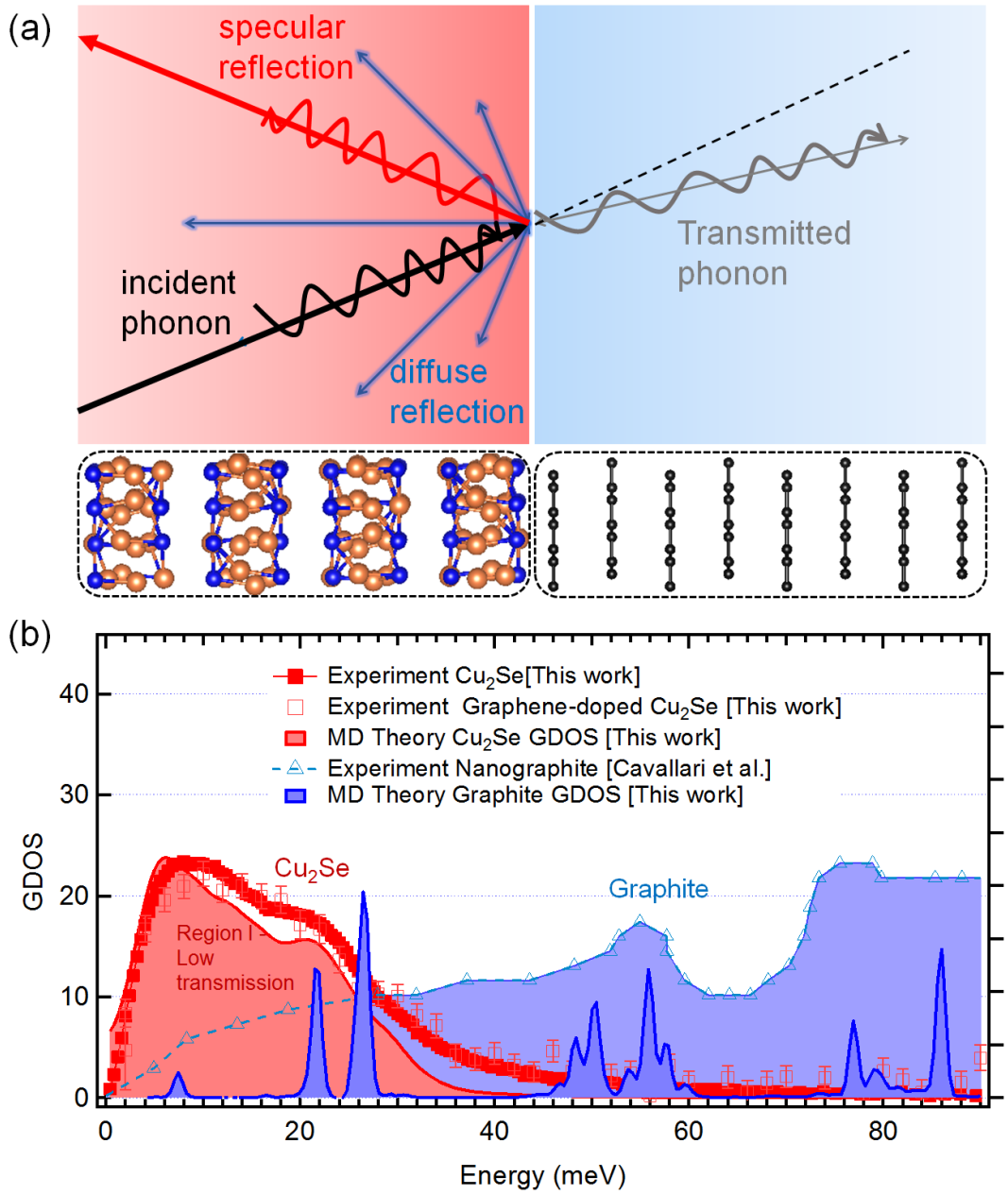

Figure 5. (a) Schematic illustration of two different scattering processes: specular reflection and diffuse scattering, for a phonon at the Cu_2Se/C interface. In diffuse scattering, the angle and momentum of the incident phonon are not correlated with the properties of the outgoing phonon, and the transmission probability is defined by the relative density of states at the phonon frequency. (b)

The density of states of Cu_2Se measured via neutron spectroscopy experiment, and calculated with *ab initio* molecular dynamics, shows high spectral weight below 30 meV. The measured and calculated density of states of graphite has a low spectral weight below 30 meV, indicating a low probability of transmission for phonons below 30 meV between Cu_2Se and graphite. At higher energies above 50 meV, the graphite has a high density of states, whereas that of Cu_2Se is negligible, indicating transmission of high-energy phonons will be forbidden using a direct one-phonon process.

Highlights

- A synthesis method is reported for graphene-incorporated Cu_2Se nanocomposites.
- Nanoplate carbon inclusions strongly reduce the thermal conductivity.
- A record high thermoelectric figure-of-merit for Cu_2Se is achieved.
- Molecular dynamic simulations are carried using density functional theory.
- The interfacial resistance is rationalized based on the diffusion mismatch model.